



Particles' distribution enhancing in aluminum-based composites produced by upward friction stir processing

Catarina Vidal^{1,2} · Pedro M. Ferreira¹ · Patrick L. Inácio¹ · Francisco B. Ferreira¹ · Duarte Santiago¹ · Pedro Meneses¹ · Rui J. C. Silva³ · Telmo G. Santos^{1,2}

Received: 19 April 2023 / Accepted: 23 May 2023
© The Author(s) 2023

Abstract

A new variant of friction stir processing named upward friction stir processing (UFSP) is a promising approach to control particles' distribution and promote a more uniform distribution over a larger processed area. This variant involves using two sheets with functional particles between them to produce metallic composites. A spacer is used to ensure the desired quantity and uniform distribution of the particles and prevent sputtering. This technique promotes an upward flow to introduce more particles with a uniform distribution in the processed volume, avoiding discrete holes or grooves. This study involved enhancing the particles' distribution by varying process parameters. The resulting trial with the best particles' distribution was characterized by means of light microscopy, eddy current testing, microhardness mapping, scanning electron microscopy, and energy-dispersive X-ray spectroscopy. The study revealed that UFSP can improve the particles' distribution in the stir zone of metallic composites, especially when multi-passes are performed towards the retreating side of the plates. The process parameters that produced an improvement in particles' distribution were six passes with an offset of 1 mm towards the retreating side, the tool rotation and processing speed of 900 rev/min, and 180 mm/min, respectively, and a spacer's thickness of 0.5 mm. The resulting hardness and electrical conductivity profiles show that the UFSP technique can significantly affect material's properties, including mechanical strength, particularly when processing with tool offset towards the retreating side. Furthermore, the hardness increased by about 22% in composites produced with the addition of reinforcement particles. However, for some aluminum alloys, the properties decreased under such conditions. These findings highlight the potential of UFSP for producing functionalized materials with tailored properties, while also underscoring the importance of careful parameters selection to optimize the material's performance.

Keywords Upward friction stir processing · Metal matrix composites · Aluminum-based matrix composites · Particles · Solid-state

Highlights

- Particles' distribution affected by upward friction stir processing was investigated.
- Advanced and mechanical characterization was performed on optimized UFSP samples.
- Particles' distribution in Al/WC in situ composite was homogenized by UFSP.

✉ Catarina Vidal
c.vidal@fct.unl.pt

¹ UNIDEMI, Department of Mechanical and Industrial Engineering, NOVA School of Science and Technology, Universidade NOVA de Lisboa, 2829-516 Caparica, Portugal

² Laboratório Associado de Sistemas Inteligentes, LASI, 4800-058 Guimarães, Portugal

³ CENIMAT/i3N, Departamento de Ciência dos Materiais, NOVA School of Science and Technology, Universidade NOVA de Lisboa, 2829-516 Caparica, Portugal

1 Introduction

For processing and welding metallic alloys, friction stir processes could be a viable alternative to fusion-based technologies because these processes have a low carbon and environmental footprint. The variants of friction stir processes are additive friction stir deposition (AFSD) [1, 2], friction stir additive manufacturing (FSAM) [3, 4], friction stir welding (FSW) [5, 6], friction stir processing (FSP) [7, 8], friction surfacing (FS) [9, 10], friction stir spot welding (FSSW) [11, 12], friction stir lap welding (FSLW) [13, 14], and friction stir vibration process (FSVP) [15–17]. The basic underlying principle of these processes is to weld/process/deposit materials using friction as a thermal energy source. Axial force, rotational speed, and weld or traverse speed are the common control parameters of all friction stir processing techniques.

Furthermore, tool profiles and tool dimensions are known to have an impact on weld or stir region quality [18].

FSP is a solid-state technique that employs the FSW principles. The FSW technique involves the use of a rotating tool to cause deformation and friction heat at the joint of two materials component [19]. FSP is used to produce ultra-fine-grained materials with improved mechanical properties. This can be done by introducing functional particles into the base material [19].

Functional materials produced by FSP, such as metal matrix composites (MMC), have been developed for traditional engineering applications, including high-specific mechanical strength and wear resistance applications [20–23]. However, if more effective stirring techniques are developed, the potential of friction stir-based processes can be extended beyond the traditional mechanical-oriented applications [24]. FSP variant techniques capable of producing these materials are thus required. FSP has been studied for MMC manufacturing, and several reinforcement methods have been documented in the literature [25].

Several particles, including titanium dioxide (TiO_2), silicon carbide (SiC) [26–29], alumina (Al_2O_3) [30, 31], titanium carbide (TiC) [32], titanium aluminum carbide (Ti_3AlC_2) [33], tungsten carbide (WC) [34, 35], and barium titanate (BaTiO_3) [36], have been widely used as reinforcement in materials to improve their mechanical and microstructural properties. The process parameters and the concentration of the reinforcing material are the primary factors that determine the properties of materials reinforced with these particles. Lower rotation speeds during the manufacturing process can also lead to finer microstructures. Overall, the use of particles as reinforcement has been found to be effective in enhancing the mechanical and microstructural properties of materials [37].

Aluminum-based matrix composites have various industrial applications and possess numerous beneficial properties including high fatigue strength, low thermal expansion, and excellent wear resistance. These materials find applications in a wide range of fields, including automobile, aerospace, rail and marine transportation, construction and building industry, and many others, owing to their excellent attributes such as high strength-to-weight ratio, exceptional tensile strength, high fracture toughness, and superior wear resistance [38–41]. The manufacturing process for AMCs typically involves combining a reinforcement material with an aluminum matrix using friction stir processing [42–44]. In general, the process includes embedding the reinforcement into a groove or holes on the surface of the metal matrix plate and then applying FSP to mix the two. The earliest known technique involves directly pasting a layer of particles mixed with methanol on the base material matrix and subsequent processing [45].

A new FSP-based alternative to produce functionalized materials incorporating any kind of solid particles was proposed by Inácio et al. [46], i.e., the upward friction stir processing (UFSP) variant. UFSP variant is a process for producing metallic composites that differs from existing variants by promoting an “aspiration” effect (upward flow) rather than bringing reinforcement particles from an upper layer to a lower one. To do this, two sheets (the bottom one of which can be a sacrificial plate) are used with functional particles between them. With this method, it is possible to introduce more particles with a more uniform distribution in the processed volume since they are continuously confined between the two sheets rather than being enclosed in discrete holes or grooves. To promote the upward flow effect, a counter clockwise rotation of the tool is necessary when using a left-hand thread pin. To ensure the desired quantity and uniform distribution of the functional particles between the two sheets, a spacer is used. In addition, the spacer also prevents sputtering of the particles [46].

The distribution of particles in metal matrix composites produced by FSP is the key factor in ensuring good mechanical properties, as clusters of particles in these composites can affect mechanical properties [47, 48]. Consequently, the production of MMCs with a homogeneous distribution of functional particles is advantageous. In this work, particles’ distribution of composites produced by the UFSP technique was improved by applying different UFSP process parameters. Additionally, the trials were carried out and characterized by means of light microscopy, eddy current testing, microhardness mapping and advanced characterization techniques, such as scanning electron microscopy (SEM) and energy-dispersive X-ray spectroscopy (EDS).

2 Materials and methods

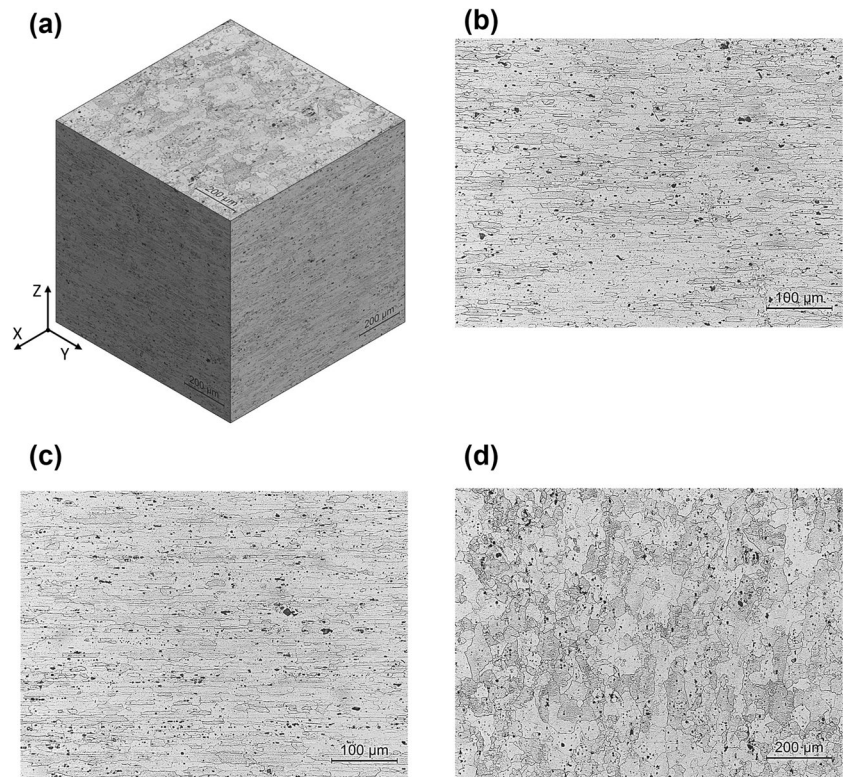
2.1 Materials

Aluminum alloys play an important role on engineering applications, mainly on those involving friction-based manufacturing technologies due to be suitable for solid-state processing. In this work, commercial AA7075–T651 plates with 203 (rolling direction) \times 103 \times 3 mm were used as base material. The average hardness measured on a polished base material sample was 180 HV0.5. The nominal composition of the Al plates is depicted in Table 1 [46].

Base material metallographic investigations were carried out to characterize the grain structure and to identify the presence of intermetallic components. The aluminum alloy used in this study is a wrought alloy, so the grain morphology depends on the metallurgical direction. In Fig. 1, it is possible to observe that this material has an anisotropic structure

Table 1 Chemical composition of aluminum alloy 7075-T651 (wt%) [46]

Elements	Al	Cr	Cu	Fe	Mg	Mn	Si	Ti	Zn
(wt%)	Remnant	0.18–0.28	1.2–2.0	0.5	2.1–2.9	0.3	0.4	0.2	5.1–6.1

Fig. 1 Base material micrography: (a) 3D grain structure; (b) micrograph showing the grain structure on the YZ plane; (c) micrograph showing the grain structure on the XZ plane; (d) micrograph showing the grain structure on the XY plane

with microstructural differences along the directions analyzed. Thus, three different planes were analyzed, i.e., YZ (Fig. 1(b)), XZ (Fig. 1(c)), and XY (Fig. 1(d)) where X, Y, and Z stand for rolling direction, long transverse, and short transverse, respectively. Optically, the grain structure on the XZ plane is composed of elongated flattened grains along the rolling direction (X direction), as shown in Fig. 1(c).

Silicon carbide (SiC) microparticles, with 99.5% of purity, were used for analyzing the effect of UFSP process parameters in the particles' distribution, even though many other functional particles can be used, depending on the desired functionality for the base material, such as, TiO₂, SiC [26–29], Al₂O₃ [30, 31], TiC [32], Ti₃AlC₂ [33], WC [34, 35], and BaTiO₃ [36]. The SiC particles were characterized by not uniform shape and the particles' size ranges between 4 and 20 µm, with an average diameter of 6 µm [46].

A composite material was produced using optimized UFSP parameters. To enhance the contrast of the composite under X-ray microtomography (µCT), tungsten carbide (WC) particles were incorporated into the composite material. WC has a higher X-ray attenuation coefficient than SiC. By incorporating WC particles with higher X-ray attenuation coefficient into the base material, the composite material can

achieve higher contrast under µCT imaging, allowing for better visualization and analysis of the internal structure of the composite material. The ability of a material to absorb X-rays is influenced by its atomic number and density, and the use of WC particles can provide better contrast for analyzing structures with higher density contrast under µCT, when compared to SiC particles. The WC particles were characterized using scanning electron microscopy (SEM), as shown in Fig. 2 (a). These particles have a granular morphology and a size smaller than 3 µm. Energy-dispersive X-ray spectroscopy (EDS) analysis confirmed the presence of tungsten (W) and carbon (C) in the particles, as seen in Fig. 2(b). The SEM used for this analysis was a ZEISS DSM 962, and a thin coating of conductive gold was applied to improve the particles' conductivity.

2.2 Methods

A set of multi-stack functionalized composites was fabricated by incorporation of SiC and WC particles within the aluminum substrate via UFSP, as described on the schematic presented in Fig. 3. Moreover, the particles were positioned only in the middle of the plates and within

Fig. 2 WC particles morphology and dimensions observed by SEM: (a) scanning electron microscopy image; (b) chemical elemental mapping determined by energy-dispersive X-ray spectroscopy

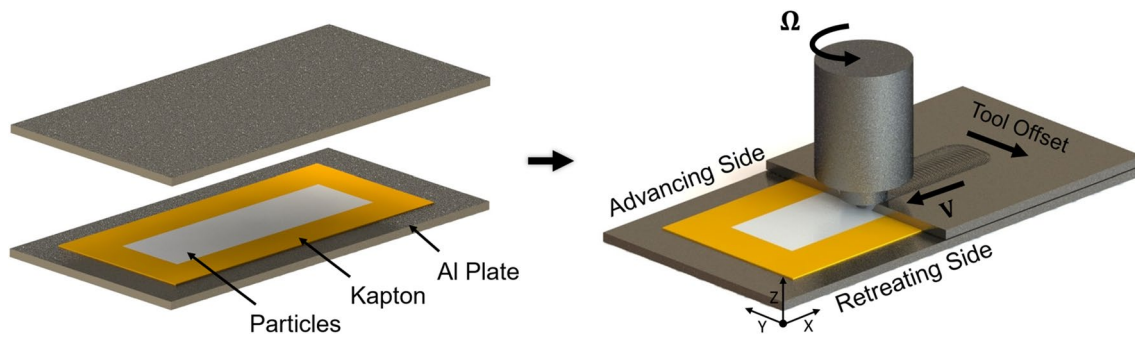
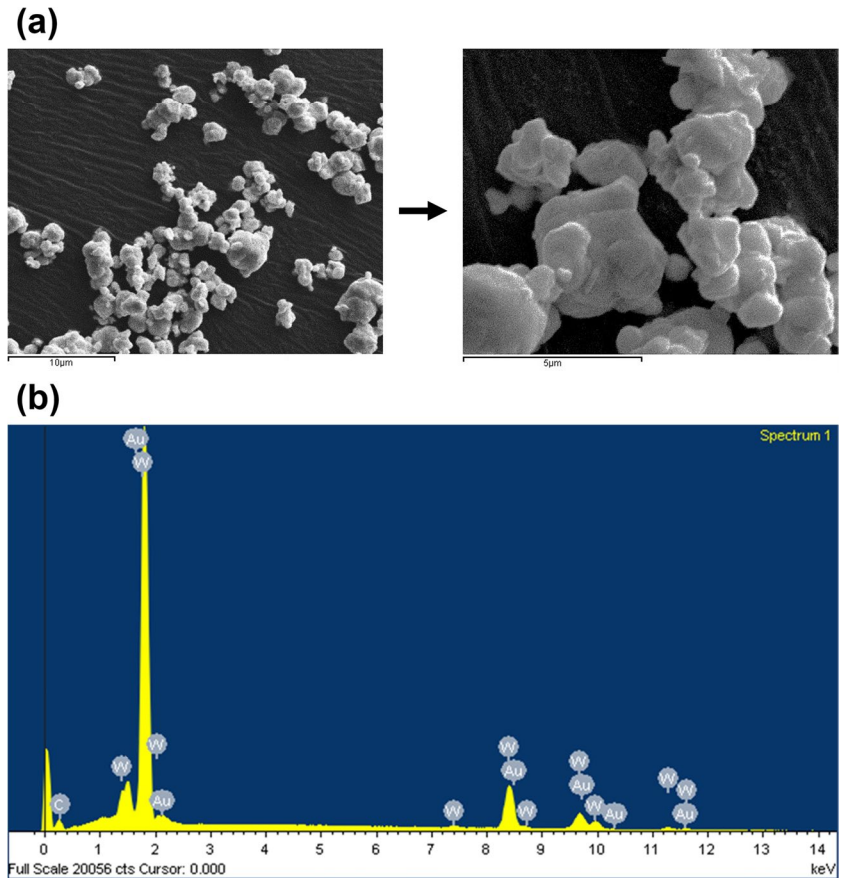


Fig. 3 Schematic representation of the Upward Friction Stir Processing (UFSP) variant

a well-defined volume measuring $150 \times 50 \times 0.5$ mm (Fig. 3). In this study, 3-mm-thick plates of aluminum alloy AA7075-T651 were used as a metal matrix. Table 2 presents the processing parameters utilized to improve the particles' distribution by UFSP technique, including the pitch ratio (Ω/V) [rev/mm], the tool rotation speed (Ω) [rev/min], the tool traveling speed (V) [mm/min], the tool offset [mm] and the spacer's thickness [mm]. These parameters were carefully chosen based on critical conditions observed during experimental trials, providing valuable insights into the optimization process.

After the processing parameters were optimized, a set of characterization techniques were used to assess the microstructural, mechanical, and electrical properties of the composites. The optimized parameters used were: six passes with an offset of 1 mm towards the retreating side (sample #WC_R) and the advancing side (sample #WC_A), the tool rotation and processing speed were 900 rev/min and 180 mm/min, respectively, and the spacer's thickness was 0.5 mm. Thus, Table 3 shows the identification of the composites manufactured. As control samples, samples without particles (samples #R and #A) were also prepared.

Table 2 The processing parameters used to optimize the UFSP technique

Sample #	Variable parameters					Constant parameters		
	Pitch ratio (Ω/V) [rev/mm]	Rotation speed (Ω) [rev/min]	Traveling speed (V) [mm/min]	Offset [mm]	Spacer's thickness [mm]	No. processing passes	Tilt angle [$^\circ$]	Tool geometry
Pitch ratio (Ω/V) influence						6	1	Triflute left-hand threaded conical probe of 5 mm of diameter and 6 mm of length
1	2.5	900	355	0.5	0.35			
2	3.1	560	180					
3	5	900	180					
4	6.8	560	90					
5	7.2	1400	180					
Tool offset influence								
3	5	900	180	0.5	0.35			
6				0.7				
7				1				
8				2				
Layer thickness influence								
7	5	900	180	1	0.35			
9					0.5			
10					0.7			
11					1			

Table 3 Composites produced to microstructural, mechanical, and electrical characterization

Sample #	Particles type	Tool offset direction
WC_R	WC	Retreating side
WC_A	WC	Advancing side
R	No particles	Retreating side
A	No particles	Advancing side

Following composites processing, samples were prepared for various characterization techniques. The macro and micrography, and μ CT samples were ground and polished according to standard metallographic procedures. Previously, the samples were sectioned along the Y direction, to reveal the stir zone. Then, macro and micrography samples were etched in Keller reagent.

Macro- and micrography analyses were performed using a Leica DMI 5000 M inverted optical microscope to reveal the microstructure and particles' distribution. A high-resolution image of the cross-section was created by taking sequential images and combining them.

The 3D and 2D micro-architectural morphology of the composites based on WC particles was characterized by μ CT, using a Phoenix V|TOME|X, GE, according to the procedure conducted by Vidal et al. [49]. The acquired image data were interpreted qualitatively and quantitatively using 3D tomographic reconstruction and

analysis software (Volume Graphics 3.04 software, Volume Graphics).

To obtain a more detailed characterization of the macro and micrography samples, scanning electron microscopy (SEM) was performed using a ZEISS DSM 962 equipment, and the corresponding X-ray energy-dispersive spectrometer (EDS) with an INCA X-act detector ($SDD = 10 \text{ mm}^2$) from Oxford Instruments was used to assess the elemental chemical composition. SEM images were recorded using secondary electrons. In addition, a thin conductive gold coating was applied to improve the conductivity of the WC particles.

For eddy current characterization and potential drop measurements, the top surface of the samples was machined down, grounded, and polished to obtain a homogenous surface condition. Microhardness profiles were also obtained on the same surface.

A Mitutoyo HM-112 hardness testing machine was used to measure the Vickers microhardness profile along the length (X direction) of the composites and processed material without particles. The spacing between consecutive indentions was of 1 mm for the base material and 0.5 mm for processed and heat/thermo-mechanically affected regions. The load used was 0.5 kgf applied for 10 s.

The electrical conductivity was characterized using eddy currents and potential drop measurement techniques. This electrical property was measured along a straight line along X direction. The procedure was developed according to Sorger et al. [50] and Santos et al. [51]. So, to obtain a homogeneous

surface of the samples, 1 mm of the top surface was machined down. A pencil probe operating at 2 MHz (corresponding to a penetration depth of 0.019 mm for this alloy) and a NORTEC 600 D impedance analyzer were used to implement the eddy currents technique. A four-point probe with four straight aligned tungsten needles with a radius of $0.4 \mu\text{m}$ was used to implement the potential drop measurement technique. A Keithley SourceMeter 2450 was used to impose 80 mA and a Keithley Nanovoltmeter 2182A was used to measure the voltage, allowing the calculation of the electrical conductivity.

3 Results and discussion

3.1 Effect of process parameters in particles' distribution

Trials were carried out to evaluate the effect of the UFSP parameters by analyzing the particles' distribution. The influence of the pitch ratio (Ω/V), tool offset and layer thickness, for the processing set up with six passes towards the retreating side, were studied and the results are presented in Fig. 4.

Five sets of processing parameters were chosen to range the pitch ratio from $\Omega/V = 2.5$ to 7.8 rev/mm (sample #1 to sample #5). It was found that a lower pitch ratio increases the arm flow towards the nugget zone and produces an asymmetrical

distribution of particles. On the other hand, a higher pitch ratio decreases the homogeneity of the composite, and an increase of the tunnel defect size was observed. The trial with a pitch ratio of 5 rev/mm , with $\Omega = 900 \text{ rev/min}$ and $V = 180 \text{ mm/min}$ (sample #3), was considered the best result since a homogenous and symmetrical composite was observed. Despite some heterogeneity found on higher pitch ratio trials, the feasibility of the process was also achieved, and it can be a way for product differentiation.

The increase of tool offset is beneficial since it increases the process productivity. This is because enlarging the spacing between successive passes provides a greater capacity for producing larger stir zones with multifunctional particles. However, it was found that lower offset increases the homogeneity in particles' distribution and a higher offset promotes heterogeneity. It was concluded that the trial with an offset of 1 mm (sample #7) was the best option.

By varying the layer thickness of the reinforcement particles, the volume fraction changes. Trials with layer thicknesses of 0.35 mm, 0.5 mm, 0.7 mm, and 1.0 mm were performed (samples #7, #9, #10, and #11, respectively). The concentration of particles decreases with lower layer thickness. The feasibility of the process is guaranteed for all layer thicknesses; however, the appearance of particles clusters in the trial with a layer thickness of 0.7 mm (sample #9) was observed, and above this layer thickness, an increase of particles clusters is expected.

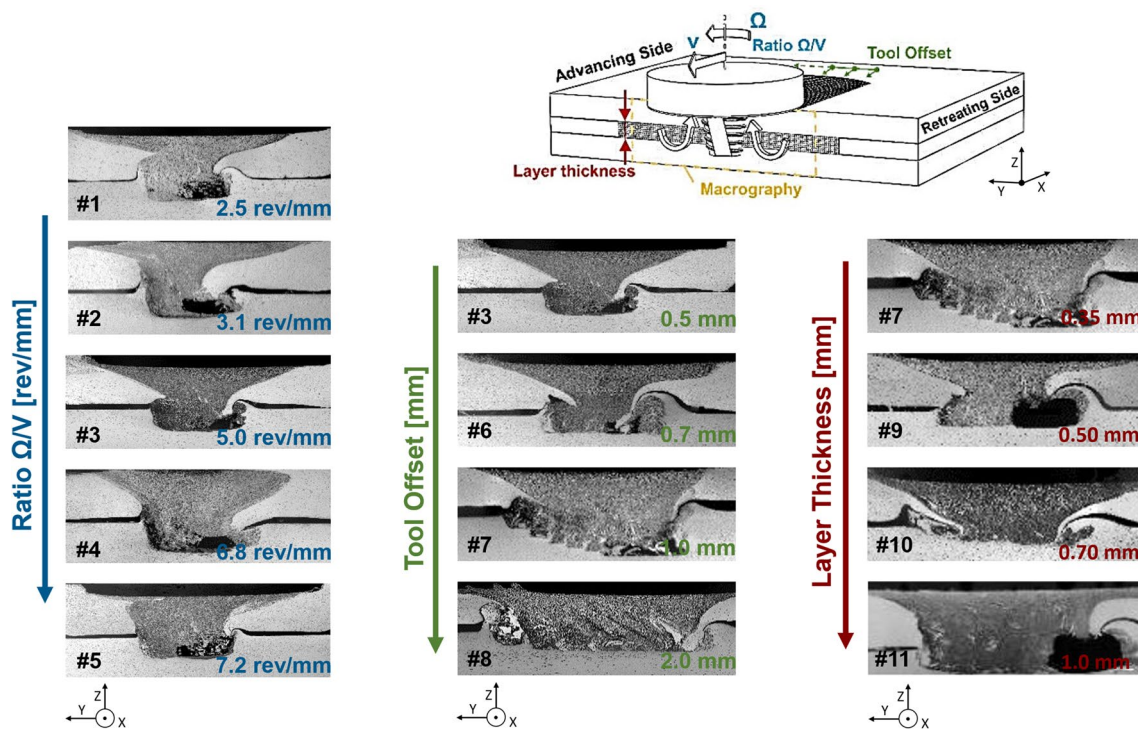


Fig. 4 Effect of UFSP process parameters in the particles' distribution: influence of the pitch ratio (Ω/V), the tool offset, and the layer thickness

Regarding the pin and the tool used, an analysis of the pin wear after successive passes was performed, as shown in Table 4. As a result, after 12 passes, the pin shows visible wear, i.e., the ascending channels are completely blocked by material, with some alterations at the thread level. After 18 passes, the pin wears out and there is an accumulation of material on the outer edge of the shoulder.

3.2 Composites characterization

3.2.1 Macro and microstructural characterization

The intense plastic deformation during FSP creates four regions: the unaffected zone (base material), the heat-affected zone (HAZ), the thermo-mechanically affected zone (TMAZ), and the dynamic recrystallisation zone or stir zone.

In all tests, the stir zone has a recrystallized microstructure of fine granulometry. The particles embedded in the composite are found in this zone, with a homogeneous distribution. Dynamic recrystallization can cause difficulties in interpreting the local textures in terms of the deformation state of the metal [52]. In the UFSP process, the microstructure's homogeneity in the stir zone is mainly influenced by dynamic recrystallization, which is governed by the applied strain. The recrystallized microstructure's homogeneity can be improved by increasing the deformation temperature and/or reducing the strain rate. This results in the nucleation of new grains in specific areas of the matrix, leading to a reduction in grain size [53]. In addition, reinforcement particles play a crucial role in the fragmentation of grains within the processed microstructure due to localized and non-uniform deformation [54]. Consequently and according to Bagheri et al. [55], it can be inferred that smaller particles have a more pronounced effect on grain refinement in the microstructure compared to larger particles during the FSP process. When temperatures close to that of recrystallization are achieved in the TMAZ, especially in a zone closer to the stir zone, the high plastic deformations that occur in the grain structure are visible. The HAZ has a slightly larger grain size and a slightly more rounded grain geometry than the TMAZ, which has grains with a more elongated geometry.

The macrographs and SEM images presented in Fig. 5 show that in all the tests, the thickness of the upper sheet in

the processed zone remains nearly the same as in the non-processed zone (approximately 3 mm), despite the presence of a very well-located defect only in the sacrificial sheet (bottom sheet).

In sample #WC_R (Fig. 5(d), (e), (f)), it was observed that the particles were more evenly distributed on the retreating side (RS) than on the advancing side (AS). On the other hand, in sample #WC_A (Fig. 5(a), (b), (c)), the inverse was observed, a more homogeneous distribution of the particles occurred in the AS rather than in the RS. When comparing these two samples, it can be seen that when the tool offset was performed towards the RS (sample #WC_R), the particles' incorporation was more homogeneous than when the tool offset was performed towards the AS (sample #WC_A). Nevertheless, sample #WC_A has a higher particles' concentration, as shown in Fig. 5 (b) when compared to Fig. 5(e).

Samples #R (Fig. 5(g), (h)) and #A (Fig. 5(i), (j)) were obtained from UFSPs performed without particles incorporation in order to be compared to samples #WC_R and #WC_A. As a result, samples #R and #A have a grain size in the dynamic recrystallization zone that is slightly larger than the grain size of samples #WC_R and #WC_A.

The μ CT analyses were conducted on samples #WC_R and #WC_A due to the relevance of evaluating the 3D distribution of particles inside composites (Fig. 6). When comparing the composites' image with the three different phases merged—the aluminum matrix (blue color), nugget (green color), and particles (red color)—within the composites, a 3D viewpoint of the particles' distribution can be viewed. The particles' distribution can be seen inside the nugget. The particles were homogeneously and spatially distributed along the processed zone, as shown in Fig. 6. Furthermore, there were no detectable voids in the processed zone. The results of μ CT analyses are consistent with macro- and microstructural analyses, i.e., when the tool offset was performed towards the RS (sample #WC_R), particles' incorporation was more homogeneous than when the tool offset was performed towards the AS (sample #WC_A).

Figure 7 presents an EDS spectrum and mapping images of the surface of sample #WC_R. The EDS spectrum in Fig. 7(a), (b) indicates the presence of Al, Mg, Zn, W, and C in the sample. With the addition of particles, W

Table 4 Effect of the tool passes on its wear




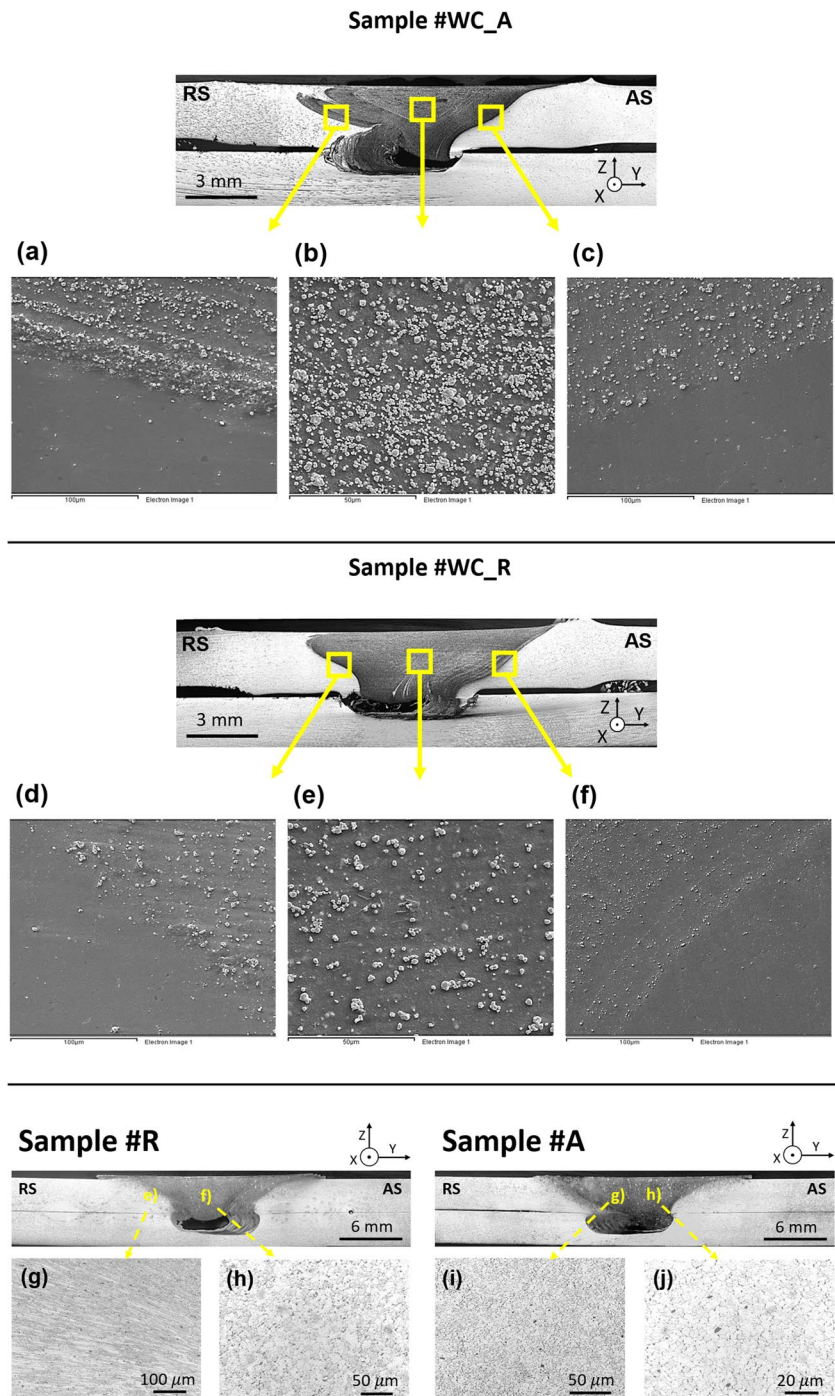
Tool Geometry	Number of Tool Passes		
	0	12	18
Triflute left-hand threaded conical probe			

Fig. 5 Metallographic results: scanning electron microscopy images of sample #WC_A (a, b, c) and sample #WC_R (d, e, f); optical microscopy images of sample #R (g, h) and sample #A (i, j)



and C are also detected. Figure 7(c), (d), (e) shows EDS mapping images that confirm the existence of Al and W in the sample. These images demonstrate the different phases and confirm the presence of elements in the surface composite. The mapping images reveal that the WC particles were incorporated in the aluminum matrix material. Furthermore, the main elements of sample #WC_R, such as Al and W, are clearly observed in the mapping images.

3.2.2 Microhardness and electrical conductivity measurements

To characterize the processed and non-processed zones and evaluate the particles' distribution, microhardness measurements and potential drop measurements were performed in the transversal section (*Y* direction) of the plates, 1 mm below the top surface. Hardness can be also an indicator

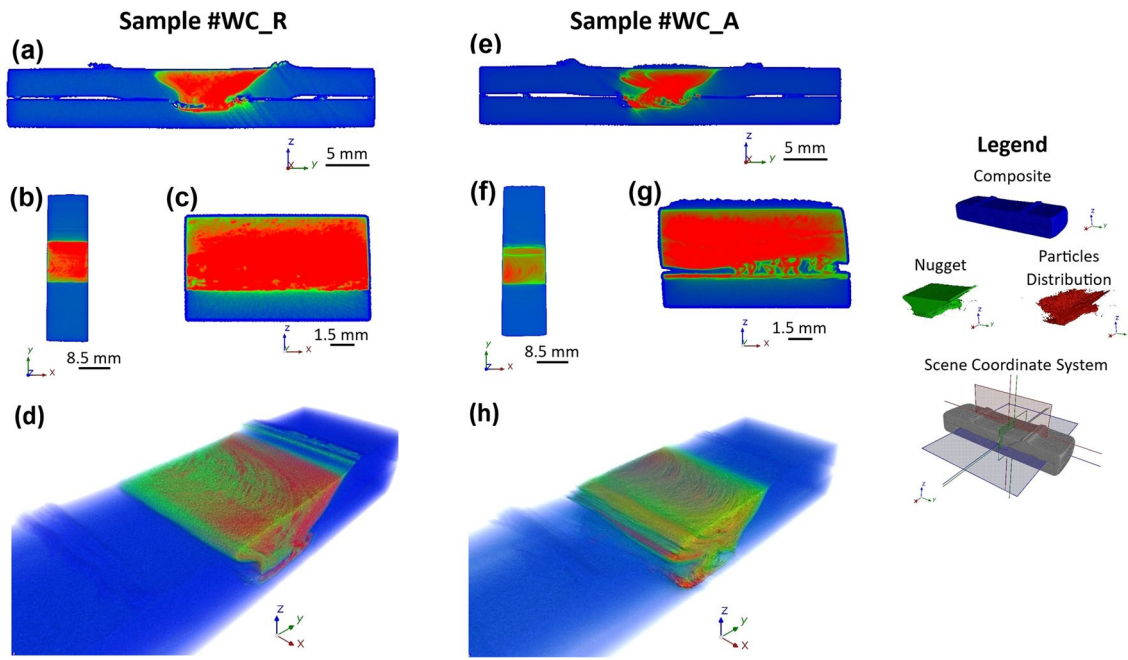
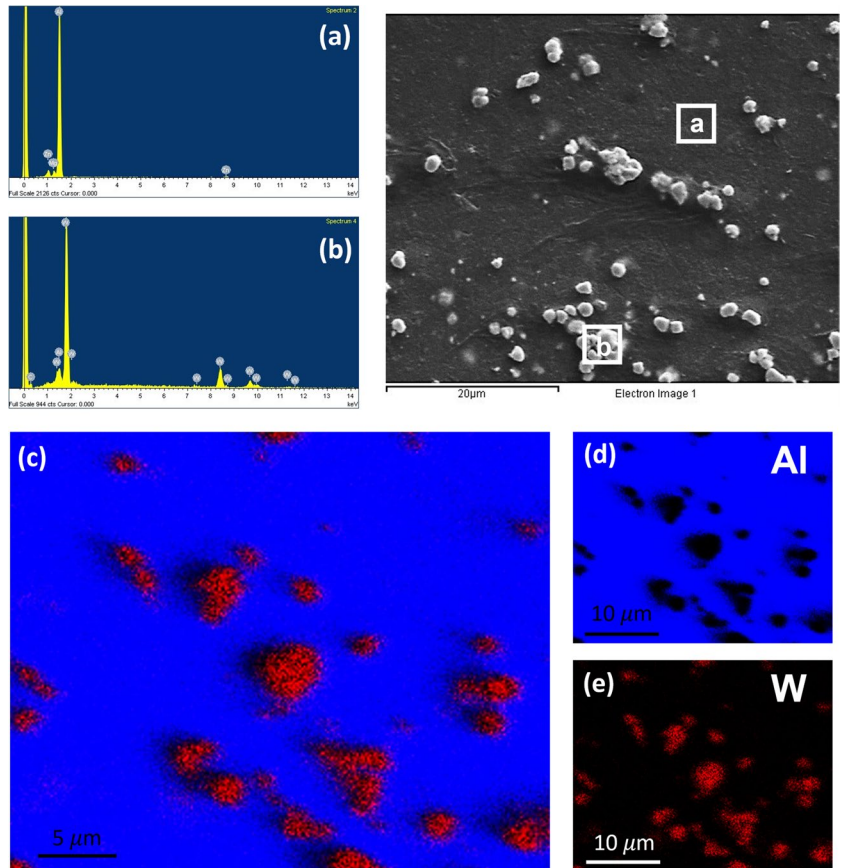


Fig. 6 3D μ CT images of samples #WC_R (a, b, c, d) and #WC_A (e, f, g, h) fabricated by UFSP. Segmented μ CT images of composites (a, b, c, e, f, g); the 3D representation of the μ CT of composites (d, h)

Fig. 7 Energy-dispersive X-ray spectroscopy (EDS) images of sample #WC_R: spectrum images of Al metallic matrix (a) and WC particles (b); mapping images (c, d, e)

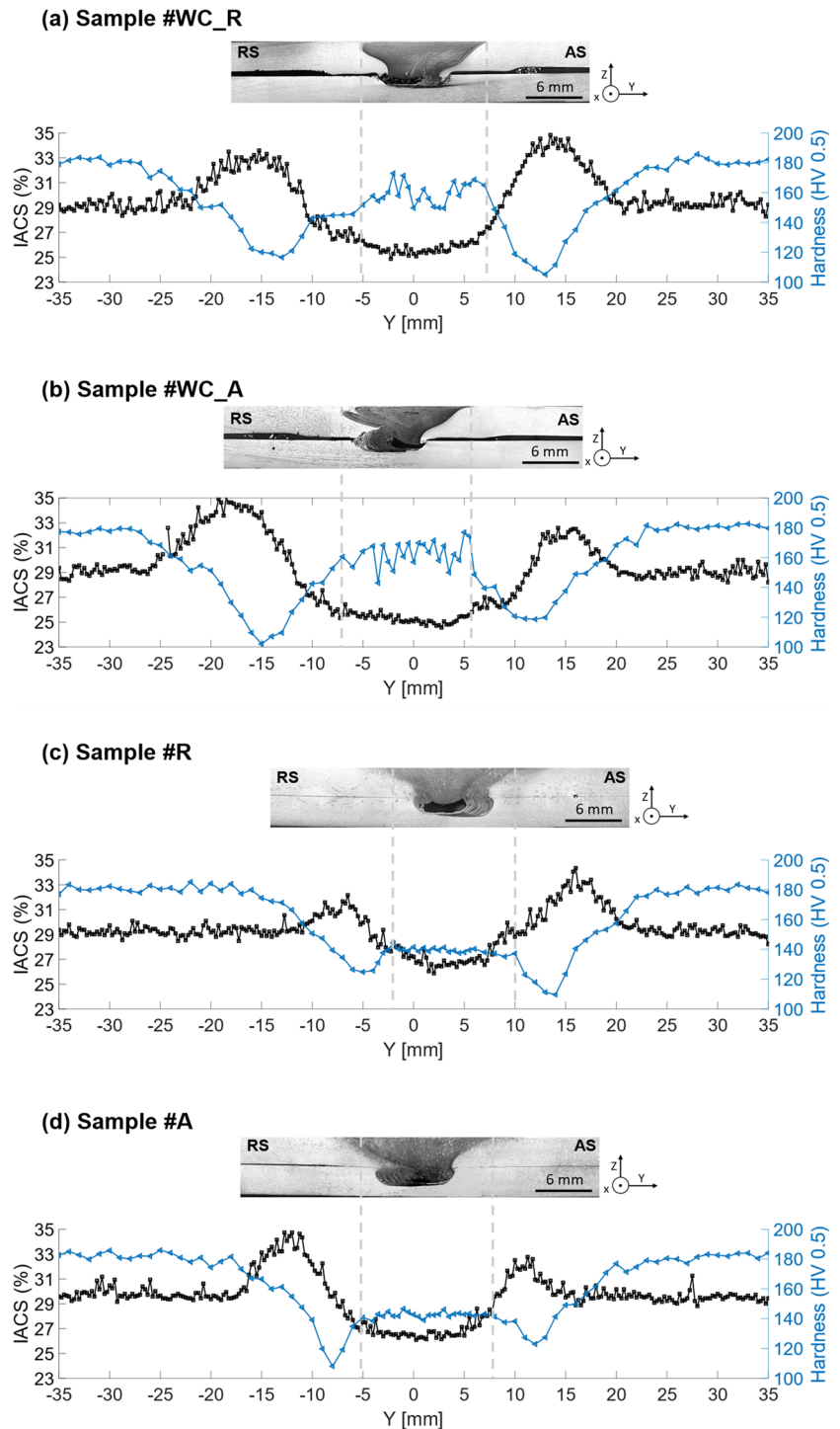


of processing conditions in terms of mechanical strength since it is directly proportional to it. Potential drop measurements allow obtain the resistivity and conductivity in processed and non-processed zones. In fact, other works have shown that electrical conductivity is inversely proportional to hardness, and thus to the mechanical strength. As such, processed zones have lower electrical conductivity, since more grain boundaries reduce the electronic mobility, while

the thermal affected zones have higher conductivity due to the grain growth [50, 51, 56, 57].

Figure 8 depicts the hardness and electrical conductivity profiles of samples #WC_R, #WC_A, #R, and #A. It is observed a slight decrease of hardness in the stir zone when compared to the base material for all samples. The hardness in the non-affected zone (base material) remains relatively constant, with an average value of 180 HV0.5. Electrical

Fig. 8 Profiles of microhardness and electrical conductivity, expressed in % of the International Annealed Copper Standard (IACS). 1%IACS is equal to 5.5×10^5 S/m



conductivity measurements are also consistent throughout this zone, with a value close to the theoretical value of 29.3% IACS for aluminum alloy 7075-T651 (Fig. 8). In the heat-affected zones, i.e., in the HAZ and TMAZ, the electrical conductivity values increase, and the hardness values decrease, since these zones present a larger grain size. Thus, the maximum values of electrical conductivity and the minimum hardness are reached in the HAZ. A low-temperature annealing experience during processing reduces the strengthening effect caused by the T651 heat treatment. However, the presence of WC particles in samples #WC_R and #WC_A (Fig. 8(a), (b)), increased the hardness in that region when compared to samples #R and #A (Fig. 8(c), (d)), respectively. Electrical conductivity measurements are in good agreement with the obtained hardness profiles.

The processing strategy for samples #WC_R and #WC_A was to offset the tool in each pass by 1 mm in the direction of the retreating and advancing sides, respectively. This aimed to assess the dispersion of WC particles in the Al matrix. According to the macrographic analysis, imposing an offset towards the advancing side promotes heterogeneity, whereas imposing an offset towards the retreating side promotes homogeneity. The hardness and electrical conductivity profiles plotted in Fig. 8 highlight this evidence even more. Inside the stir zone, sample #WC_R has a maximum hardness of 173 HV0.5, whereas sample #WC_A has a uniform plateau hardness level of \approx 168 HV0.5.

Figure 8(c), (d) depicts the macrostructure, microhardness, and electrical conductivity profiles of the samples produced without particles, corresponding to samples #R and #A. Both hardness and electrical conductivity profiles have a symmetrical-like form, which is consistent with what was expected for this configuration without WC particles. When compared to the results obtained for the samples with WC particles, the mechanical strength of the stir zone is at a lower level as the base material level.

The results of hardness and electrical conductivity profiles previously described demonstrate that the UFSP variant can affect material properties, including the mechanical strength, particularly when processing with the tool offset towards the retreating side.

4 Conclusions

The recent developed solid-state processing variant, named UFSP, proved to be a highly effective method for producing customized materials with incorporated functional particles. In addition, the experimental setup and parameters optimization carried out, enabled the achievement of precise localization of defects exclusively in the bottom plate, while maintaining the thickness of the upper

plate nearly unchanged. The process parameters that produced an improvement in the particles' distribution were six passes with an offset of 1 mm towards the retreating side, a tool rotation and processing speed of 900 rev/min and 180 mm/min, respectively, and a spacer's thickness of 0.5 mm. Furthermore, when employing UFSP with multi-passes towards the retreating side, plates exhibited a more uniform dispersion of reinforcement particles within the stir zone. Additionally, this zone revealed a finer grain size when processed with reinforcement particles compared to processing without them.

The stir zone presented higher microhardness and lower electrical conductivity after processing with reinforcement particles compared to processing without them. Specifically, composites produced with WC particles showed a 6% reduction in hardness, while composites without reinforcement particles experienced a 22% reduction, when compared to the base material. Moreover, the electrical conductivity decreased by approximately 11% for composites produced without reinforcement particles and by about 18% for composites produced with WC particles, also when compared to the base material.

The optimized UFSP variant proved to be effective in producing customized aluminum-based matrix composites with functional particles incorporated, enhanced dispersion of reinforcement particles, finer grain size in the stir zone, and improved microhardness and electrical conductivity properties.

Acknowledgements The authors would like to thank Micronsense-Metrologia Industrial (Leiria, Portugal) for the μ CT analysis.

Funding Open access funding provided by FCTIFCCN (b-on). CV and TGS acknowledge Fundação para a Ciência e a Tecnologia (FCT-MCTES) for its financial support via projects UIDB/00667/2020 and UIDP/00667/2020 (UNIDEMI). PMF also acknowledges FCT-MCTES for its financial support via the PhD scholarship UI/BD/151055/2021. PLI would like to acknowledge FCT-MCTES for its financial support via the PhD scholarship FCT-SFRH/BD/146885/2019. RJCS acknowledges national funds from FCT-MCTES, in the scope of the project UIDB/50025/2020–2023 of the CENIMAT/i3N.

Declarations

Ethics approval The authors declare that the present study is original, without any kind of plagiarism and/or inappropriate data manipulation/falsification form and has not been divided in several parts. The authors also declare that the work reported in this paper has not been published previously, and is not under consideration for publication elsewhere, in English or in any other language.

Consent to participate Not applicable.

Consent for publication The authors declare that they consent the publication of the work reported in this paper.

Competing interests The authors declare no competing interests.

Open Access This article is licensed under a Creative Commons Attribution 4.0 International License, which permits use, sharing, adaptation, distribution and reproduction in any medium or format, as long as you give appropriate credit to the original author(s) and the source, provide a link to the Creative Commons licence, and indicate if changes were made. The images or other third party material in this article are included in the article's Creative Commons licence, unless indicated otherwise in a credit line to the material. If material is not included in the article's Creative Commons licence and your intended use is not permitted by statutory regulation or exceeds the permitted use, you will need to obtain permission directly from the copyright holder. To view a copy of this licence, visit <http://creativecommons.org/licenses/by/4.0/>.

References

1. Srivastava M, Rathee S, Maheshwari S, Noor Siddiquee A, Kundra TK (2019) A review on recent progress in solid state friction based metal additive manufacturing: friction stir additive techniques. *Crit Rev Solid State Mater Sci* 44:345–377. <https://doi.org/10.1080/10408436.2018.1490250>
2. Gopan V, Leo Dev Wins K, Surendran A (2021) Innovative potential of additive friction stir deposition among current laser based metal additive manufacturing processes: a review. *CIRP J Manuf Sci Technol* 32:228–248. <https://doi.org/10.1016/j.cirpj.2020.12.004>
3. Lu IK, Reynolds AP (2021) Innovative friction stir additive manufacturing of cast 2050 Al–Cu–Li aluminum alloy. *Prog Addit Manuf* 6:471–477. <https://doi.org/10.1007/S40964-021-00175-5/FIGURES/14>
4. Palanivel S, Nelaturu P, Glass B, Mishra RS (2015) Friction stir additive manufacturing for high structural performance through microstructural control in an Mg based WE43 alloy. *Mater Des* 65:934–952. <https://doi.org/10.1016/j.matdes.2014.09.082>
5. Delijaicov S, Rodrigues M, Farias A, Neves MD, Bortolussi R, Miyazaki M et al (2020) Microhardness and residual stress of dissimilar and thick aluminum plates AA7181-T7651 and AA7475-T7351 using bobbin, top, bottom, and double-sided FSW methods. *Int J Adv Manuf Technol* 108:277–287. <https://doi.org/10.1007/s00170-020-05370-2>
6. Kumar Rajak D, Pagar DD, Menezes PL, Eyvazian A (2020) Friction-based welding processes: friction welding and friction stir welding. *J Adhes Sci Technol* 34:2613–2637. <https://doi.org/10.1080/01694243.2020.1780716>
7. Mironov S, Sato YS, Kokawa H (2008) Microstructural evolution during friction stir-processing of pure iron. *Acta Mater* 56:2602–2614. <https://doi.org/10.1016/j.actamat.2008.01.040>
8. Barmouz M, Givi MKB (2011) Fabrication of in situ Cu/SiC composites using multi-pass friction stir processing: Evaluation of microstructural, porosity, mechanical and electrical behavior. *Compos Part A Appl Sci Manuf* 42:1445–1453. <https://doi.org/10.1016/j.compositesa.2011.06.010>
9. Gandra J, Pereira D, Miranda RM, Vilaça P (2013) Influence of process parameters in the friction surfacing of AA 6082-T6 over AA 2024-T3. *Procedia CIRP*, vol. 7, Elsevier, p 341–6. <https://doi.org/10.1016/j.procir.2013.05.058>
10. Gandra J, Krohn H, Miranda RM, Vilaça P, Quintino L, Dos Santos JF (2014) Friction surfacing - a review. *J Mater Process Technol* 214:1062–1093. <https://doi.org/10.1016/j.jmatprotec.2013.12.008>
11. Ayaz A, Ülker A (2021) Effects of process parameters on the lap joint strength and morphology in friction stir spot welding of ABS sheets. *J Elastomers Plast* 53:612–631. <https://doi.org/10.1177/0095244320961525>
12. Labus Zlatanovic D, Balos S, Bergmann JP, Köhler T, Grätzel M, Sidjanin L et al (2020) An experimental study on lap joining of multiple sheets of aluminium alloy (AA 5754) using friction stir spot welding. *Int J Adv Manuf Technol* 107:3093–3107. <https://doi.org/10.1007/s00170-020-05214-z>
13. Geng P, Ma Y, Ma N, Ma H, Aoki Y, Liu H et al (2022) Effects of rotation tool-induced heat and material flow behaviour on friction stir lapped Al/steel joint formation and resultant microstructure. *Int J Mach Tools Manuf* 174:103858. <https://doi.org/10.1016/j.ijmactools.2022.103858>
14. Das H, Basak S, Das G, Pal TK (2013) Influence of energy induced from processing parameters on the mechanical properties of friction stir welded lap joint of aluminum to coated steel sheet. *Int J Adv Manuf Technol* 64:1653–1661. <https://doi.org/10.1007/s00170-012-4130-3>
15. Bagheri B, Abbasi M, Abdollahzadeh A, Kokabi AH (2020) A comparative study between friction stir processing and friction stir vibration processing to develop magnesium surface nanocomposites. *Int J Miner Metall Mater* 27:1133–1146. <https://doi.org/10.1007/s12613-020-1993-4>
16. Bagheri B, Abdollahzadeh A, Sharifi F, Abbasi M, Moghaddam AO (2021) Recent development in friction stir processing of aluminum alloys: microstructure evolution, mechanical properties, wear and corrosion behaviors. *Proc Inst Mech Eng Part E J Process Mech Eng*:095440892110580. <https://doi.org/10.1177/09544089211058007>
17. Abdollahzadeh A, Bagheri B, Abbasi M, Sharifi F, Ostovari-Moghaddam A (2021) Mechanical, wear and corrosion behaviors of AZ91/SiC composite layer fabricated by friction stir vibration processing. *Surf Topogr Metrol Prop* 9:035038. <https://doi.org/10.1088/2051-672X/ac2176>
18. Prabhakar DAP, Shettigar AK, Herbert MA, Patel GCM, Pimenov DY, Giasin K et al (2022) A comprehensive review of friction stir techniques in structural materials and alloys: challenges and trends. *J Mater Res Technol* 20:3025–3060. <https://doi.org/10.1016/j.jmrt.2022.08.034>
19. Mirzadeh H (2021) High strain rate superplasticity via friction stir processing (FSP): a review. *Mater Sci Eng A* 819:141499. <https://doi.org/10.1016/j.msea.2021.141499>
20. Singh L, Singh B, Saxena KK (2020) Manufacturing techniques for metal matrix composites (MMC): an overview. *Adv Mater Process Technol* 6:441–457. <https://doi.org/10.1080/2374068X.2020.1729603>
21. Gandra J, Miranda RM, Vilaça P (2011) Effect of overlapping direction in multipass friction stir processing. *Mater Sci Eng A* 528:5592–5599. <https://doi.org/10.1016/j.msea.2011.03.105>
22. Gandra J, Vigarinho P, Pereira D, Miranda RM, Velhinho A, Vilaça P (2013) Wear characterization of functionally graded Al–SiC composite coatings produced by friction surfacing. *Mater Des* 52:373–383. <https://doi.org/10.1016/j.matdes.2013.05.059>
23. Jain VKS, Yazar KU, Muthukumar S (2019) Development and characterization of Al5083-CNTs/SiC composites via friction stir processing. *J Alloys Compd* 798:82–92. <https://doi.org/10.1016/j.jallcom.2019.05.232>
24. Santos TG, Lopes N, Machado M, Vilaça P, Miranda RM (2015) Surface reinforcement of AA5083-H111 by friction stir processing assisted by electrical current. *J Mater Process Technol* 216:375–380. <https://doi.org/10.1016/j.jmatprotec.2014.10.005>
25. Mishra R, Ma Z, Charit I (2003) Friction stir processing: a novel technique for fabrication of surface composite. *Mater Sci Eng A* 341:307–310. [https://doi.org/10.1016/S0921-5093\(02\)00199-5](https://doi.org/10.1016/S0921-5093(02)00199-5)
26. El-Mahallawy NA, Zoalfakar SH, Abdel Ghaffar Abdel Maboud A (2019) Microstructure investigation, mechanical properties and wear behavior of Al 1050/SiC composites fabricated by friction stir processing (FSP). *Mater Res Express* 6:096522. <https://doi.org/10.1088/2053-1591/ab2ce2>

27. Huang C, Li W, Zhang Z, Fu M, Planche MP, Liao H et al (2016) Modification of a cold sprayed SiCp/Al5056 composite coating by friction stir processing. *Surf Coatings Technol* 296:69–75. <https://doi.org/10.1016/j.surfcoat.2016.04.016>
28. Butola R, Tyagi L, Singari RM, Murtaza Q, Kumar H, Nayak D (2021) Mechanical and wear performance of Al/SiC surface composite prepared through friction stir processing. *Mater Res Express* 8:016520. <https://doi.org/10.1088/2053-1591/abd89d>
29. Mehdi H, Mishra RS (2022) Consequence of reinforced SiC particles on microstructural and mechanical properties of AA6061 surface composites by multi-pass FSP. *J Adhes Sci Technol* 36:1279–1298. <https://doi.org/10.1080/01694243.2021.1964846>
30. Mazaheri Y, Karimzadeh F, Enayati MH (2011) A novel technique for development of A356/Al₂O₃ surface nanocomposite by friction stir processing. *J Mater Process Technol* 211:1614–1619. <https://doi.org/10.1016/j.jmatprotec.2011.04.015>
31. Shafiei-Zarghani A, Kashani-Bozorg SF, Hanzaki AZ (2011) Wear assessment of Al/Al₂O₃ nano-composite surface layer produced using friction stir processing. *Wear* 270:403–412. <https://doi.org/10.1016/j.wear.2010.12.002>
32. Shojaeefard MH, Akbari M, Asadi P, Khalkhali A (2017) The effect of reinforcement type on the microstructure, mechanical properties, and wear resistance of A356 matrix composites produced by FSP. *Int J Adv Manuf Technol* 91:1391–1407. <https://doi.org/10.1007/s00170-016-9853-0>
33. Ahmadifard S, Momeni A, Bahmanzadeh S, Kazemi S (2018) Microstructure, tribological and mechanical properties of Al7075 / Ti₃AlC₂ MAX-phase surface composite produced by friction stir processing. *Vacuum* 155:134–141. <https://doi.org/10.1016/j.vacuum.2018.06.002>
34. Huang G, Hou W, Shen Y (2018) Evaluation of the microstructure and mechanical properties of WC particle reinforced aluminum matrix composites fabricated by friction stir processing. *Mater Charact* 138:26–37. <https://doi.org/10.1016/j.matchar.2018.01.053>
35. Huang G, Wu J, Hou W, Shen Y, Gao J (2019) Producing of Al–WC surface composite by additive friction stir processing. *Mater Manuf Process* 34:147–158. <https://doi.org/10.1080/10426914.2018.1532590>
36. Ferreira PM, Machado MA, Carvalho MS, Vidal C (2023) Granting sensorial properties to metal parts through friction stir processing. *Measurement* 207:112405. <https://doi.org/10.1016/j.measurement.2022.112405>
37. Zass K, Mabuwa S, Msomi V (2022) A review on reinforced particles used on the production of FSP composites. *Mater Today Proc* 56:2392–2397. <https://doi.org/10.1016/j.matpr.2021.12.210>
38. Tang S, Ummethala R, Suryanarayana C, Eckert J, Prashanth KG, Wang Z (2021) Additive manufacturing of aluminum-based metal matrix composites—a review. *Adv Eng Mater* 23:2100053. <https://doi.org/10.1002/adem.202100053>
39. Pawar PB, Wabale RM, Utpat AA (2018) A comprehensive study of aluminum based metal matrix composites: challenges and opportunities. *Mater Today Proc* 5:23937–23944. <https://doi.org/10.1016/j.matpr.2018.10.186>
40. Kumar Sharma A, Bhandari R, Aherwar A, Rimašauskienė R, Pinca-Bretotean C (2020) A study of advancement in application opportunities of aluminum metal matrix composites. *Mater Today Proc* 26:2419–2424. <https://doi.org/10.1016/j.matpr.2020.02.516>
41. Ferreira PM, Machado MA, Carvalho MS, Vidal C (2022) Embedded sensors for structural health monitoring: methodologies and applications review. *Sensors* 22. <https://doi.org/10.3390/s2218320>
42. Selvakumar S, Dinaharan I, Palanivel R, Babu BG (2017) Development of stainless steel particulate reinforced AA6082 aluminum matrix composites with enhanced ductility using friction stir processing. *Mater Sci Eng A* 685:317–326. <https://doi.org/10.1016/j.msea.2017.01.022>
43. Vijayavel P, Balasubramanian V (2017) Effect of pin profile volume ratio on microstructure and tensile properties of friction stir processed aluminum based metal matrix composites. *J Alloys Compd* 729:828–842. <https://doi.org/10.1016/j.jallcom.2017.09.117>
44. Dursun T, Soutis C (2014) Recent developments in advanced aircraft aluminium alloys. *Mater Des* 56:862–871. <https://doi.org/10.1016/j.matdes.2013.12.002>
45. Sharma V, Prakash U, Kumar BVM (2015) Surface composites by friction stir processing: a review. *J Mater Process Technol* 224:117–134. <https://doi.org/10.1016/j.jmatprotec.2015.04.019>
46. Inácio PL, Nogueira F, Ferreira FB, Vidal C, Schell N, Tero T et al (2022) Functionalized material production via multi-stack Upward Friction Stir Processing (UFSP). *Mater Manuf Process* 37:11–24. <https://doi.org/10.1080/10426914.2021.1942909>
47. Kundurti SC, Sharma A, Tambe P, Kumar A (2022) Fabrication of surface metal matrix composites for structural applications using friction stir processing – a review. *Mater Today Proc* 56:1468–1477. <https://doi.org/10.1016/j.matpr.2021.12.337>
48. Mohamadigangaraj J, Nourouzi S, Jamshidi Aval H (2021) The effect of heat treatment and cooling conditions on friction stir processing of A390–10 wt% SiC aluminium matrix composite. *Mater Chem Phys* 263:124423. <https://doi.org/10.1016/j.matchemphys.2021.124423>
49. Vidal C, Alves P, Alves MM, Carmezim MJ, Fernandes MH, Grenho L et al (2022) Fabrication of a biodegradable and cytocompatible magnesium/nanohydroxyapatite/fluorapatite composite by upward friction stir processing for biomedical applications. *J Mech Behav Biomed Mater* 129:105137. <https://doi.org/10.1016/j.jmbbm.2022.105137>
50. Sorger GL, Oliveira JP, Inácio PL, Enzinger N, Vilaça P, Miranda RM et al (2019) Non-destructive microstructural analysis by electrical conductivity: comparison with hardness measurements in different materials. *J Mater Sci Technol* 35:360–368. <https://doi.org/10.1016/j.jmst.2018.09.047>
51. Santos TG, Miranda RM, Vilaça P, Teixeira JP, dos Santos J (2011) Microstructural mapping of friction stir welded AA 7075–T6 and AlMgSc alloys using electrical conductivity. *Sci Technol Weld Join* 16:630–635. <https://doi.org/10.1179/1362171811Y.0000000052>
52. Bagheri B, Alizadeh M, Mirsalehi SE, Shamsipur A, Abdollahzadeh A (2022) The effect of rotational speed and dwell time on Al/SiC/Cu composite made by friction stir spot welding. *Weld World* 66:2333–2350. <https://doi.org/10.1007/s40194-022-01376-4>
53. Abdollahzadeh A, Bagheri B, Shamsipur A (2022) Development of Al/Cu/SiC bimetallic nano-composite by friction stir spot welding. *Mater Manuf Process*:1–10. <https://doi.org/10.1080/10426914.2022.2157435>
54. Abbasi M, Bagheri B, Sharifi F (2021) Simulation and experimental study of dynamic recrystallization process during friction stir vibration welding of magnesium alloys. *Trans Nonferrous Met Soc China* 31:2626–2650. [https://doi.org/10.1016/S1003-6326\(21\)65681-9](https://doi.org/10.1016/S1003-6326(21)65681-9)
55. Bagheri B, Shamsipur A, Abdollahzadeh A, Mirsalehi SE (2023) Investigation of SiC nanoparticle size and distribution effects on microstructure and mechanical properties of Al/SiC/Cu composite during the FSSW process: experimental and simulation. *Met Mater Int* 29:1095–1112. <https://doi.org/10.1007/s12540-022-01284-8>
56. Santos T, Vilaça P, Quintino L (2008) Developments in NDT for detecting imperfections in friction stir welds in aluminium alloys. *Weld World* 52:30–37. <https://doi.org/10.1007/BF03266666>
57. Machado MA, Rosado LS, Santos TG (2022) Shaping eddy currents for non-destructive testing using additive manufactured magnetic substrates. *J Nondestruct Eval* 41:1–11. <https://doi.org/10.1007/s10921-022-00882-1>